Nanoscale

PAPER

View Article Online
View Journal



Cite this: DOI: 10.1039/d5nr05509a

# Evaluating the efficiency of touch-spun scaffolds in producing dense cell cultures for tissue engineering applications

Kristina Peranidze, [a,b] Mikhail Parker, [a,b] Mohammad Aghajohari, [a,b] Polina Vertegel, [a,b] Sergei Makaev, [a,b] Nataraja Sekhar Yadavalli, [c] Sergiy Minko *[a,b,c] and Vladimir Reukov *[a]

Developing efficient scaffolds for long-term cell cultivation remains a challenge in tissue engineering. Biomimetic approaches aim to create a three-dimensional (3D) extracellular matrix (ECM)-like fiber network with a tunable hierarchical structure to promote sufficient cell attachment, differentiation, and overall viability. Among the fiber fabrication methods documented in the literature, mechanical fiber drawing techniques, such as touch-spinning, have garnered significant research interest. This is due to the simplicity of the equipment, the ability to control fiber diameter and interfiber spacing at the nanoscale without the need for external fields, and the absence of specific requirements for material dielectric properties. Despite the advantages of mechanically drawn scaffolds in biomedical research, the methodologies for cell culturing and analysis for these materials have not been adequately addressed. In this study, we assess the potential of touch-spun scaffolds in promoting NIH/3T3-GFP fibroblast cell growth for tissue engineering applications. Polycaprolactone/polyethylene oxide (PCL/PEO)-based fiber arrays with a controlled interfiber spacing of 91.9 ± 25.0 μm ($N$ = 50) were fabricated using a modified touch-spinning apparatus and then assembled into 2D and 3D scaffolds through additive manufacturing technology. A comparative cell analysis conducted for single- and multi-layered structures showed that the 3D touch-spun scaffolds support healthy growth of up to 6.5 million fibroblast cells within 21 days and offer enhanced cell viability compared to conventional 2D fiber scaffolds, as confirmed by the Presto Blue assay. Furthermore, the metabolic activity of fibroblasts on 3D scaffolds assessed by the MTT test is approximately four times higher than that of the positive control, making the 3D touch-spun materials ideal for long-term cell culture applications.

Received 31st December 2025,
Accepted 20th February 2026

DOI: 10.1039/d5nr05509a

rsc.li/nanoscale



## 1. Introduction

The fabrication of polymer-based fiber scaffolds with adjustable structural features has emerged as a leading strategy in the cell culturing practices of tissue engineering.[1–3] Key structural characteristics of fiber patterns that must be managed during the fabrication process include fiber diameter, interfiber spacing, fiber alignment, and crystallinity, all of which contribute to the overall mechanical properties of the final material.[4] An additional tool in enhancing cell adhesion and interaction within the polymer matrix is related to developing 3D structures that resemble the ECM down to the nanoscale.[5,6] Compared to conventional 2D fiber mats, 3D scaffolds significantly improve mechanobiology by providing an additional direction for transmitting mechanical signals from the surrounding matrix to the cells. As highlighted by Kular *et al.*,[7] communication between cells and the ECM occurs through focal adhesions – complexes of cytoskeletal and regulatory proteins that serve as both mechanical links between cell actin bundles and the fibers, as well as signaling hubs for transmitting forces and signals *via* integrins. Research has shown that in 3D fiber scaffolds, cells respond more efficiently to these signals. This leads to a faster rearrangement of their cytoskeletal structure and an increased production of natural ECM.[8,9] Therefore, 3D fiber scaffolds hold great promise for enhancing cell–matrix interactions.

The principles of fiber fabrication that allow for moderate control over the structural characteristics have been applied in various techniques, including electrospinning (ES),[10,11] magnetic field-assisted spinning,[12] mechanical drawing,[13–17] and gravity fiber drawing.[18,19] Nevertheless, many of these methods struggle to produce precise fiber patterns due to material and process limitations, and they are often incompati-

[a]*Textiles, Merchandising and Interiors, University of Georgia, Athens, GA 30605, USA. E-mail: sminko@uga.edu, Reukov@uga.edu*
[b]*Nanostructured Materials Laboratory, University of Georgia, Athens, GA 30602, USA*
[c]*CytoNest, Inc., 425 River Road, Athens, GA 30602, USA*

ble with modern additive manufacturing (AM) technologies for assembling fibers into 3D multi-layered structures. For instance, among the ES techniques that are currently prevalent in tissue engineering research, only those employing a direct writing approach – such as melt ES[20] and near-field ES[21] – can achieve adequate control over fiber arrangement. Recent advancements in mechanical fiber drawing, involving touch-spinning[16] and spinneret-based tunable engineered parameter (STEP) methods,[14,15,17] have opened new opportunities in 3D scaffold manufacturing. These methods provide effective ways to create highly aligned fiber arrays with uniform fiber diameters and consistent interfiber spacing by using programmable motor systems that control both the rotational and translational motion of spinnerets and/or collecting substrates. As a result, the limitations of the ES process, which are typically linked to the use of high voltages, can be overcome. This enables the processing of a wide variety of synthetic and natural polymers with no requirements for their dielectric properties. In this study, we utilize a modified touch-spinning apparatus to develop nano- and microfiber arrays intended for use in 3D scaffolding.

Tokarev *et al.*[16] first introduced the touch-spinning technique in 2015 as an alternative to conventional ES methods. This technique is based on a straightforward principle: the coaxial stretching of a solution droplet.[22] As the droplet is extruded through the syringe tip, it comes into contact with a rotating rod, which stretches the filament around a collecting frame of a specified shape. The frame, in turn, performs translational (*Z*-axis) motion at a speed controlled by a stepper motor, resulting in a defined spacing between the deposited fibers. Research on the touch-spinning device revealed the opportunities for fabricating fibers with diameters ranging from 40 to 5000 nm and interfiber spacing as small as 5.8 ± 1.0 μm. Despite its simple design and adaptability to large-scale manufacturing, the touch-spinning technique has not been widely discussed in the literature. Only a few research papers have examined its potential for generating materials for biomedical research, mainly concentrating on nerve[23–25] and muscle tissue regeneration,[26–28] where the alignment of the matrix fibers is essential for directing cell differentiation. Thus, the touch-spun scaffolds have been successfully applied to culture mouse neuroepithelial cells (NE-4C),[25] mouse myoblast cells (C2C12),[27,28] and NIH/3T3 mouse fibroblast cells.[29]

The existing research on cell culturing methodologies and cell analysis performed for cell lines on touch-spun materials remains incomplete. This gap hampers the evaluation of the efficiency of touch-spun scaffolds as potential substrates for producing dense cell cultures. The current study aims to assess the capabilities of 2D and 3D touch-spun scaffolds toward cell growth and establish patterns of cell activity by culturing NIH/3T3-GFP mouse fibroblasts. The GFP-marked fibroblast cells were selected as the cell model to enhance visualization. Additionally, fibroblasts are known to secrete and organize the ECM, which provides structural support for their adhesion and migration.[30,31] This allows for observation of the ECM formation process between adjacent fibers and facilitates the study of changes in cell morphology.

This study showcases a modified touch-spinning technique used to fabricate aligned fiber arrays with tunable diameters and interfiber spacing. The research compares the efficiency of 2D and 3D touch-spun scaffolds through three main analyses: (i) cell counting to determine the maximum number of cells that can be supported by the scaffold; (ii) cell viability and metabolic activity assays to confirm healthy cell growth; and (iii) cell protein quantification as an additional measure of cell response to external stimuli.

## 2. Materials and methods

### 2.1. Materials

Polycaprolactone (PCL; number-average molecular weight $M_n$ = 80 × $10^3$ Da; Sigma-Aldrich), polyethylene oxide (PEO; viscosity-average molecular weight $M_v$ = 5 × $10^6$ Da; Sigma-Aldrich), and chloroform (purity ≥ 99.8%; Thermo Fisher Scientific) were used in this study to prepare solutions for fiber spinning and spin coating. Square-shaped microscope cover glasses (22 × 22 mm; VWR International, LLC) were used as substrates for spin coating of polymer solutions. Acrylonitrile butadiene styrene filaments (ABS; diameter $d$ = 1.75 mm; Hatchbox, Inc.) with extrusion temperatures of 210–240 °C were employed for 3D printing of collecting frames and scaffold outer frames. 3D-printed PCL spacers (outer diameter $D$ = 25 mm, inner diameter $d$ = 19 mm) were provided by CytoNest, Inc. The following materials were utilized for cell culture experiments: NIH/3T3-GFP mouse fibroblasts (Cell Biolabs, Inc.), Dulbecco's Modification of Eagle's Medium with 4.5 g $L^{-1}$ glucose, L-glutamine, and sodium pyruvate (DMEM; Corning, Inc.), fetal bovine serum (FBS; RMBIO, LLC.), antibiotic–antimycotic solution (100×, stabilized; Sigma-Aldrich), phosphate buffer solution (PBS; Corning, Inc.), 0.25% trypsin–EDTA solution (Thermo Fisher Scientific), surface-treated standard tissue culture flasks T25 and T75 (growth area $s$ = 25 and 75 $cm^2$, respectively; VWR International, LLC), 6-well suspension culture plates (well diameter $d$ = 35 mm; Greiner Bio-One International GmbH), 6-well surface-treated standard tissue culture plates (well diameter $d$ = 35 mm; VWR International, LLC). 4% paraformaldehyde in PBS (Thermo Fisher Scientific), Triton X-100 (Sigma-Aldrich), rhodamine phalloidin (Thermo Fisher Scientific), and Hoechst 33258 solution (Sigma-Aldrich) were applied for cell staining for actin and nuclei. Handheld automated cell counter Scepter 3.0 (Sigma-Aldrich) with 40 μm sensors was used for cell counting. The following reagents were applied for cell analysis: PrestoBlue™ cell viability reagent (Thermo Fisher Scientific), 3-(4,5-dimethyl-2-thiazolyl)-2,5-diphenyl-2*H*-tetrazolium bromide solution (MTT; Sigma-Aldrich), dimethyl sulfoxide (DMSO; Sigma-Aldrich), Coomassie Brilliant Blue G-250 dye (Bio-Rad Laboratories, Inc.), bovine serum albumin (BSA; Thermo Fisher Scientific).

### 2.2. Scaffold fabrication

Working PCL/PEO solutions for fiber spinning and spin coating were prepared in sealed 20 mL vials using chloroform as the solvent. The solutions were stirred using a magnetic stirrer (400–500 rpm) at ~20 °C for up to 5 h. The weight fractions of PCL and PEO in the blends were 5 wt% and 0.25 wt%, respectively, corresponding to optimal spinning conditions established in previous experiments. A rheological characterization of the working PCL/PEO solution is provided in the SI (see the Materials section and Fig. S1). Reference spinning solutions of pure PCL were prepared in chloroform at a concentration of 8 wt% following the same procedure.

Within the framework of this study, three groups of materials were fabricated from PCL/PEO solutions: (i) polymer films on glass substrates ('flat surfaces'); (ii) single-layer fiber scaffolds; and (iii) 3D (multilayer) fiber scaffolds. The first group may serve as a reference for the second and third groups, while the second group may serve as a reference for the third group in assessing scaffold efficiency for dense cell culture development. In addition, fiber arrays composed of pure PCL were fabricated to compare fiber morphology with that of PCL/PEO fibers.

**Spin coating of PCL/PEO solutions.** To prepare PCL/PEO films on glass substrates, square-shaped coverslips were thoroughly washed with 70% ethanol (Lab Alley, LLC), dried under a directed air stream, and plasma-treated in high-power mode (30 W, ~0.5–0.6 Torr) for 60 s using a PDC-001-HP expanded plasma cleaner (Harrick Plasma, Thermo Fisher Scientific). The working PCL/PEO solutions, diluted tenfold, were then spin-coated onto the coverslips using a Smart Coater SC110-B (Best Tools, LLC) at 4000 rpm for 40 s. The applied droplet volume was 100 μL per sample. Due to the high evaporation rate of chloroform, extended spin-coating times were unnecessary. Prepared 'flat surfaces' were placed in 6-well suspension culture plates and subjected to plasma post-treatment in high-power mode for 30 s.

**Touch-spinning of PCL/PEO and PCL solutions.** PCL/PEO and PCL fiber arrays used for the fabrication of single-layer and 3D fiber scaffolds were produced using a modified, homemade touch-spinning apparatus (CytoNest, Inc.). The touch-spinning device employed in this research was originally introduced in our review article[32] and subsequently adapted for the fabrication of biomimetic 3D scaffolds for insulin-producing INS-1 cell cultures.[33] Related apparatus based on similar mechanical drawing principles has also been reported by Uddin *et al.* for the fabrication of polyhydroxybutyrate fibrous scaffolds.[34] In this study, the touch-spinning device employs rotational motion of the spinneret around a fiber-collecting frame and translational (*Z*-axis) motion of the frame driven by a programmable stepper motor (Fig. 1a). Polymer solution is delivered to the system *via* a syringe connected to a syringe pump. Upon extrusion of a solution droplet through a 22G syringe needle, the rotating spinneret contacts the droplet and stretches it into a thin nano- or microfilament. As the solvent evaporates, the filament solidifies and is deposited onto a

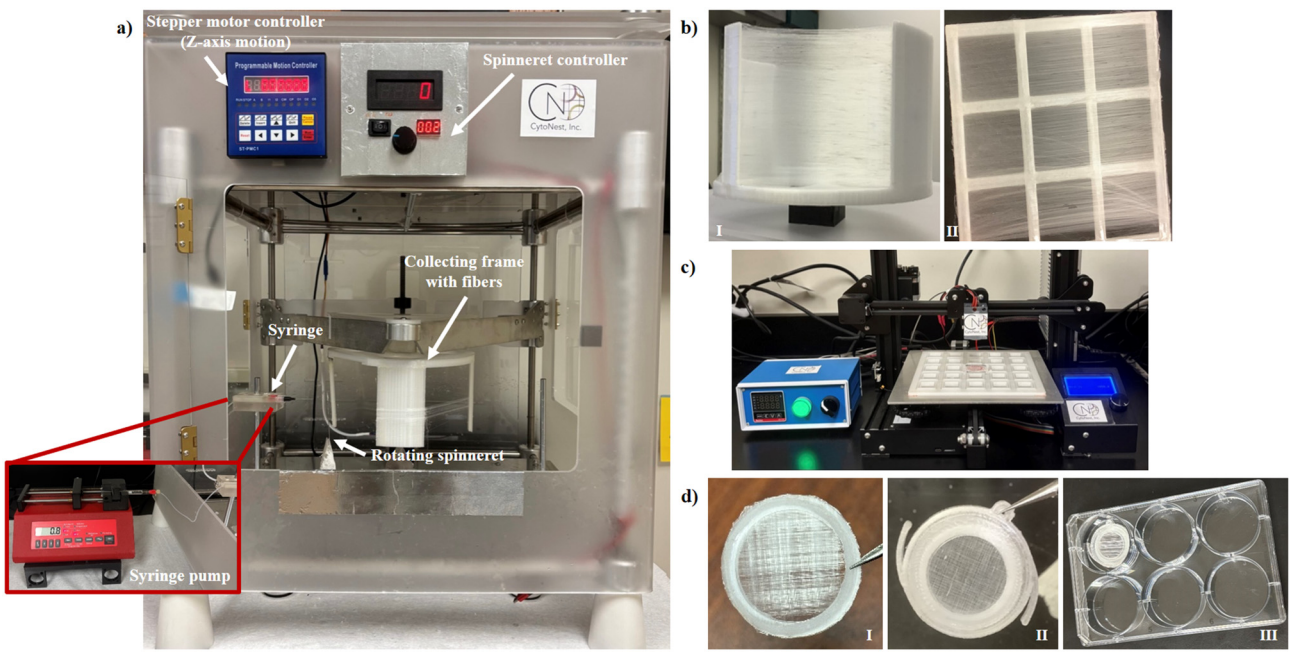


**Fig. 1** Touch-spinning of PCL/PEO and PCL solutions: (a) touch-spinning device (CytoNest, Inc.) equipped with a programmable stepper motor and spinneret speed controller; (b) four-sectioned fiber-collecting frame with deposited fibers (I) and a smaller nine-sectioned collecting frame (II); (c) heat press machine (CytoNest, Inc.) used to assemble collected fibers into circular fragments using PCL-based spacers; (d) 3D scaffold fabricated by stacking three fiber layers at 90° (I), 3D scaffold with outer 3D-printed ABS frames (II), and 3D scaffold positioned in a well of a 6-well suspension culture plate for post-treatment (III).

white, four-sectioned fiber-collecting frame (Fig. 1bI), covering all sections of the frame.

In addition to solution and environmental parameters that must be optimized for the spinning process,[35] the key technological parameters include the solution feed rate (pump rate), the rotational speed of the spinneret, and the *Z*-axis speed of the frame. The latter determines the interfiber distance in the resulting fiber array. The major solution, technological, and environmental touch-spinning parameters used for the fabrication of all groups of fiber scaffolds are summarized in Table 1.

**Assembly of fiber arrays into scaffolds.** In this study, a 3D-printed ABS frame with four sections for fiber deposition (Fig. 1bI) was used as the primary collector. For subsequent fiber collection and assembly into single-layer and multilayer structures, a smaller 3D-printed nine-sectioned ABS frame (Fig. 1bII) was placed onto each collector section containing intact fiber arrays. Fibers collected on the smaller frame were then cut into circular fragments using 3D-printed PCL spacers and a heat press device (CytoNest, Inc.) operating at 90 °C (Fig. 1c). The spacer dimensions were intentionally matched to the dimensions of the heating element, while the smaller frame dimensions were matched to the device platform. During this process, each fiber layer was sandwiched between two spacers, which were fused together under the heat press for 3–5 s. Preparation of a single-layer fiber scaffold requires two spacers and a single fusion step. Additional fiber layers can be incorporated by stacking a previously prepared single layer with a second fiber array at a selected orientation, followed by spacer fusion. Using this approach, we manufactured a series of single-layer touch-spun fiber scaffolds and 3D scaffolds comprising three orthogonally aligned fiber layers. An illustration of the 3D scaffold is presented in Fig. 1dI. For improved handling during subsequent cell research conducted in 6-well plates, researchers at CytoNest, Inc. developed custom ABS-based outer frames to stabilize the scaffolds when placed in wells with culture medium. An illustration of the scaffold with the outer frames, as well as its positioning within a 6-well plate, is shown in Fig. 1dII and dIII, respectively.

All samples underwent plasma treatment in high-power mode for 60 s, performed within 4 h prior to cell seeding. Before application, the nine-sectioned collecting frames and ABS outer frames were UV-treated (UVP Crosslinker CL-3000L; Analytik Jena US, LLC) for 15 min.

### 2.3. Scaffold characterization

**Fiber arrangement.** The initial assessment of fiber arrangement and alignment within the touch-spun fiber arrays was performed on single- and two-layer scaffolds using an optical microscope (Olympus BX51; Evident Scientific, Inc.) equipped with a high-resolution camera (Andor iXon3; Oxford Instruments, plc). The magnifications used were 20×, 50×, and 100×.

A more detailed characterization of fiber diameter, interfiber spacing, and other morphological properties of PCL/PEO fibers was carried out based on single- and two-layer structures using a variable-pressure scanning electron microscope (Hitachi SU-3900 SEM; Hitachi High-Tech, Inc.) operated at 10 kV and 30 Pa in backscattered electron (BSE) mode. A field emission scanning electron microscope (FEI Teneo, Thermo Fisher Scientific) equipped with a concentric backscattered detector (CBS) was used to examine reference PCL fiber patterns at an operating voltage of 5 kV. For SEM studies, the specimens were gently attached to stubs using 12 mm carbon conductive tabs, ensuring the original fiber arrangement was preserved. The specimens were then coated with a 20 nm layer of Au/Pd nanoparticles using a sputter coater (EM ACE600; Leica Microsystems, Inc.).

Additional characterization of PCL/PEO fiber morphology was performed using atomic force microscopy (AFM). Fibers were fixed onto silicon wafers using Anycubic UV-curable resin. A thin resin layer (~200–300 nm) was spin-coated onto the wafer surface, which was then gently brought into contact with the fibers. The resin was cured under UV illumination to secure the fibers in place. AFM imaging was performed using a Dimension Icon microscope (Bruker) equipped with a TAP-300 probe (resonant frequency ~300 kHz, spring constant ~40 N m$^{-1}$, nominal tip radius ~10 nm) to scan fiber bundles.

Fiber diameter and interfiber spacing were analyzed using ImageJ software.

**Fiber crystalline structure.** In this study, we aimed to investigate the crystalline structure of touch-spun PCL/PEO fibers using powder X-ray diffraction (XRD). Diffraction patterns were collected using a D2 PHASER diffractometer (Bruker) with Cu Kα ($\lambda$ = 1.54059 Å) radiation over a 2$\theta$ range of 5–65°, with a step size of 0.02°. Sample preparation involved mounting dense fiber arrays onto square glass substrates using

**Table 1** Touch-spinning parameters

| Material | Polymer fraction, wt% | Feed rate, mL h$^{-1}$ | Rotational speed[a], rpm | Tangential speed[b], m s$^{-1}$ | *Z*-axis speed, steps[c] | Humidity, % | Temperature, °C |
|---|---|---|---|---|---|---|---|
| PCL/PEO fibers for single-layer scaffolds | 5/0.25 | 0.4 | ~160–180 | 2.1 | 10 | 34 | 24.0–24.5 |
| PCL/PEO fibers for 3D scaffolds | 5/0.25 | 0.4 | ~160–180 | 2.1 | 10 | 38 | 18.8–21.9 |
| Reference PCL fibers | 8 | 0.1 | ~140–180 | 2.0 | 25 | 35 | 23.2–23.6 |

[a] The rotational speed of the spinneret is sensitive to mechanical fluctuations in the system; therefore, the speed was maintained within a controlled range. [b] The tangential speed during fiber spinning was determined according to $v = 2\pi Nr/60$, where $N$ represents the median rotational speed (rpm) and $r$ denotes the rotation radius, taken as 0.12 m. [c] For this touch-spinning apparatus, 10 and 25 steps correspond to a translational speed of ~40 and 100 mm h$^{-1}$, respectively.

 

double-sided adhesive tape. Based on the obtained XRD patterns, crystallite sizes were calculated using the Debye-Scherrer equation:

$$\langle L\rangle_{hkl} = K\lambda/\beta\cos(\theta) \quad (1)$$

where $\langle L\rangle_{hkl}$ is the crystallite size as estimated from the ($hkl$) reflection planes, $K$ = 0.89 is the shape factor, $\lambda$ = 1.54059 Å is the wavelength of Cu Kα radiation, $\beta$ is the full width at half maximum (FWHM) of the diffraction peak determined by Gaussian fitting in Origin software, and $\theta$ is half of the measured diffraction angle.

To complement the crystalline structure analysis obtained by XRD, we evaluated the degree of fiber crystallinity *via* differential scanning calorimetry (DSC). DSC analysis was performed on a PerkinElmer DSC 8000 calorimeter (PerkinElmer, Inc.) using 4 mg (±10%) of the collected PCL/PEO and reference PCL fibers. A heat–cool–heat cycle was carried out over a temperature range of −75 to 300 °C at a heating/cooling rate of 10 °C $min^{-1}$ under a $N_2$ atmosphere. Data from the first heating were used to calculate the degree of crystallinity according to the following equation:

$$\%\,\text{Crystallinity} = \Delta H_m \times 100\%/\Delta H_m^\circ \quad (2)$$

where $\Delta H_m$ is the enthalpy of fusion determined from the peak area, and $\Delta H_m^\circ$ is the reference enthalpy of fusion for a fully crystalline sample. The reference enthalpies of fusion for 100% crystalline PCL and PEO are 139.5 J $g^{-1}$ (ref. 36) and 213 J $g^{-1}$,[37] respectively.

**Fiber thermal stability.** Within this study, thermogravimetric analysis (TGA) was performed to evaluate the thermal stability of touch-spun PCL/PEO and reference PCL fibers. 7 mg (±10%) of each sample was analyzed using a PerkinElmer TGA 8000 instrument (PerkinElmer, Inc.). Measurements were carried out over a temperature range of 25–800 °C at a heating rate of 10 °C $min^{-1}$ under the $N_2$ atmosphere.

### 2.4. Scaffold efficiency assessment

**Cell culture.** Prior to seeding onto scaffolds and control wells, NIH/3T3-GFP fibroblasts were cultured to full confluency in T25 and T75 tissue culture flasks containing DMEM supplemented with 20% FBS and 2% antibiotic–antimycotic solution. Cell cultures were maintained in an incubator at 37 °C under a humidified atmosphere containing 5% $CO_2$. The culture medium was replaced every other day. To prepare fibroblasts for seeding, the culture medium was removed from the flask, and the cells were washed twice with PBS. For cell detachment, a 0.25% trypsin–EDTA solution was added to the flask, which was then incubated at 37 °C for 3–5 min under the 5% $CO_2$ atmosphere. After trypsinization, fresh culture medium was added to the flask, and the resulting cell suspension was collected into a 15 mL tube for centrifugation at 1500 rpm for 5 min to obtain a cell pellet. The trypsin-containing medium was then gently removed from the tube using a glass pipette connected to a vacuum pump. The cell pellet was resuspended in a calculated volume of fresh culture medium. A 100 μL aliquot of the cell suspension was taken for cell counting.

For seeding cells onto predominantly plasma-treated scaffolds in 6-well plates, we employed a 'dry' method: scaffolds were kept dry, a small concentrated volume of cell suspension was applied directly onto the scaffold surface, and the plate was incubated for 20 minutes to allow proper cell adhesion. For control wells, 'flat surfaces', and single-layer scaffolds, 0.5 mL of cell suspension was added, whereas for 3D scaffolds, 1 mL of cell suspension was used. Following the incubation, fresh medium was added to each well. We monitored the cells on scaffolds every other day throughout the duration of the study for imaging and cell analysis.

In this study, we conducted two independent cell culture experiments: (I) culturing NIH/3T3-GFP fibroblasts seeded at equal density on three groups of materials (2.2. Scaffold fabrication) over a predefined period, and (II) culturing NIH/3T3-GFP fibroblasts seeded at equal density on three groups of materials until full confluency was observed using an optical microscope. In the first experiment, fibroblasts were seeded at a density of ~$3.8 \times 10^5$ cells per well and monitored over a 10-day period. The primary purpose of this experiment was to evaluate cell viability, metabolic activity, and cell protein levels. In the second experiment, we aimed to determine the maximum capacity of the scaffolds to support a large number of healthy cells without forming necrotic cores. Thus, fibroblasts were seeded at a density of ~$5 \times 10^5$ cells per well, and the duration of cell growth was determined for each group of materials by optical microscopy.

**Cell visualization.** Cell growth was monitored using an optical fluorescence microscope (EVOS M5000; Thermo Fisher Scientific) equipped with GFP, DAPI, and RFP filter cubes. For the evaluation of cell growth on 3D scaffolds at later time points, a confocal laser scanning microscope (LSM 900; Carl Zeiss) was employed. As cell proliferation becomes more extensive within the 3D structures, observations using a standard optical microscope are hindered after 5–7 days of culture.

For improved visualization, fibroblasts were stained for actin filaments and nuclei following a standard staining protocol, which included cell fixation with paraformaldehyde and subsequent membrane permeabilization using a 0.1% Triton X-100 solution. Actin and nuclei were stained with rhodamine phalloidin (1 : 1000 dilution in PBS) and Hoechst 33258 (1 : 2000 dilution in PBS), respectively. After staining, the scaffolds were left in PBS for 30 min, and imaging was performed in a dark room.

**Cell counting.** To evaluate the capacity of the scaffolds to support NIH/3T3-GFP fibroblast growth in the first experiment, cell numbers were calculated based on a standard calibration curve obtained for an MTT test (Fig. S2, SI).

In the second experiment, cell counts were obtained *via* trypsinization, a standard method for cell detachment that utilizes trypsin enzyme to cleave cell protein links to surfaces.[38] Triplicate scaffolds of each group were analyzed. Before trypsinization, the outer frames of the touch-spun fiber scaffolds were gently removed using tweezers, and all samples were

transferred to new 6-well suspension culture plates to ensure that cell counts were obtained only from the scaffolds. After removal of the culture medium, each scaffold was washed twice with 2 mL of PBS, and a small volume of trypsin was applied directly to the cell-seeded material. For 'flat surfaces', 0.5 mL of trypsin was applied, whereas for single- and multilayer touch-spun scaffolds, 1 mL was used. Trypsinization was carried out for 5 min at 37 °C under the 5% $CO_2$ atmosphere. PBS, in a volume twice that of the applied trypsin, was then added to each well, and remaining cells were mechanically detached from the scaffolds with intense pipette flow. The obtained cell suspensions were transferred to 15 mL tubes and centrifuged at 1500 rpm for 5 min. Subsequently, 100 μL of each suspension was taken for cell counting using an automated cell counter. Cell counts were then normalized to the total volume of the cell suspensions.

**Cell viability and metabolic activity.** NIH/3T3-GFP fibroblast viability for 'flat surfaces', single-layer scaffolds, and 3D scaffolds was evaluated in the first experiment on day 3, 5, 7, and 10 using the PrestoBlue assay, a non-destructive resazurin-based method. Triplicate samples were analyzed for each scaffold group. Cells seeded in surface-treated 6-well plates (~$3.8 \times 10^5$ cells per well) were used as the positive control, and pure culture medium served as the negative control. The calibration curve for the assay was generated prior to analysis using a serial dilution experiment with cells seeded at densities ranging from $1.5 \times 10^3$ to $1 \times 10^5$ cells per well.

At each time point, the scaffolds were transferred to new 6-well suspension culture plates, with 3 mL of fresh medium added to each well for the PrestoBlue assay. Purple PrestoBlue solution was added to each well at 9 vol% of the total medium volume, followed by incubation for 2.5 h. Reagent–cell interaction was visually confirmed by a color change from purple to pink at the end of incubation. To assess the efficiency of interaction, we transferred 200 μL aliquots to a 96-well plate and measured fluorescence using a multimode microplate reader (Varioskan LUX; Thermo Fisher Scientific) at excitation/emission wavelengths of 560 nm/590 nm.

NIH/3T3-GFP fibroblast metabolic activity for 'flat surfaces', single-layer scaffolds, and 3D scaffolds was evaluated on day 10 of the first experiment using the MTT test. Triplicate samples were analyzed for each scaffold group, with the same control groups employed as in the cell viability assessment. The calibration curve for the assay was generated prior to the MTT test.

Since the MTT reagent terminates cell growth, the assay was performed at the end of cell culture. The 'flat surfaces' and touch-spun scaffolds without outer frames were transferred to new 6-well suspension culture plates, with 3 mL of fresh medium added per well. The MTT solution was prepared by dissolving yellow 3-(4,5-dimethyl-2-thiazolyl)-2,5-diphenyl-2*H*-tetrazolium bromide crystals in PBS at a concentration of 0.5 mg $mL^{-1}$. The MTT solution was added to each well at 10 vol% of the total medium volume, and the plates were incubated for 5 h. At the end of incubation, we observed the formation of purple formazan crystals, which were then dissolved in 3 mL of DMSO per well over 2 h in the dark. Aliquots of 200 μL were transferred to a 96-well plate, and absorbance was measured at 570 nm using a multimode plate reader.

In the second experiment investigating long-term cell growth, the MTT test results exceeded the plate reader's measurement range when the same MTT protocol was followed.

**Cell protein quantification.** Cell protein concentrations for the three scaffold groups were assessed on day 10 of the first experiment using the Bradford assay. Samples were prepared in triplicate, with cells seeded in empty wells serving as the positive control and deionized water as the negative control. Concentrations were calculated using a standard calibration curve (Fig. S2, SI) obtained for BSA dilutions in deionized water (0.2–0.8 μg $\mu L^{-1}$).

As another cell growth-terminating method, the Bradford assay was performed at the end of the cell culture. For the analysis, individual scaffolds were placed into 15 mL tubes: for 'flat surfaces', polymer films with NIH/3T3-GFP fibroblasts were carefully detached from glass substrates; and for touch-spun scaffolds, outer frames were removed. 5 mL of diluted Coomassie Brilliant Blue dye (dye : $H_2O$ = 1 : 4) was added to each tube, and the tubes were centrifuged at 1000 rpm for 5 min. Upon addition of the protein-binding dye, the sample solutions changed color almost instantly from brown to intense blue. 200 μL aliquots were collected from each tube to measure absorbance at 595 nm.

# 3. Results and discussion

## 3.1. Characterization of morphological, crystalline, and thermal properties of PCL/PEO fiber patterns

In this study, we fabricated three PCL/PEO-based sample configurations to evaluate the efficiency of 3D touch-spun scaffolds in supporting dense cell culture development: polymer films on glass substrates, single-layer touch-spun scaffolds, and 3D (multilayer) touch-spun scaffolds. Polymer films serving as conventional 2D cell culture platforms were fabricated *via* spin coating. A modified touch-spinning apparatus based on the mechanical fiber-drawing principle was used to create PCL/PEO fiber arrays with uniform fiber diameters and controlled interfiber spacing, which were then assembled into 2D and 3D fiber scaffolds using an additive manufacturing approach. As the touch-spinning technique relies strongly on solution concentration (wt%), solution feed rate (mL $h^{-1}$), and spinneret rotational speed (rpm), we employed parameters previously established in our laboratory to achieve stable spinning of continuous fiber arrays from PCL, PEO, and their blend solutions.[16,23] The *Z*-axis speed was chosen assuming that the resulting interfiber distance would fall within the range of 50–100 μm, creating a scaffold architecture favorable for fibroblast proliferation. The specific parameters used in this work for fiber spinning are summarized in Table 1.

 

A series of reference pure PCL fiber arrays was manufactured to compare their morphological, crystalline, and thermal properties with those of the studied materials. Touch-spinning from PCL/PEO solutions follows a 'stable jet' approach,[39] as the addition of the high-molecular-weight component (PEO) improves viscoelasticity and stabilizes the liquid thread during its stretching. In contrast, spinning from pure PCL solutions is less efficient, often leading to fiber breakage and the formation of a solid polymer deposit at the needle tip due to faster chloroform evaporation. Thus, the *Z*-axis speed was increased to 100 mm $h^{-1}$ to reduce the collection of broken fibers, while the feed rate was decreased to 0.1 mL $h^{-1}$ to prevent frequent needle clogging.

SEM analysis of fiber morphology indicates that the PCL/PEO fiber arrays fabricated under the selected touch-spinning parameters predominantly exhibit microscale diameters, with an average fiber diameter of 1.9 ± 0.4 μm ($N$ = 100) and an interfiber spacing of 91.9 ± 25.0 μm ($N$ = 50). SEM micrographs of two orthogonally aligned microfiber layers, along with the corresponding fiber diameter distribution, are presented in Fig. 2a and d. SEM micrographs reveal that, instead of being deposited individually with spacing, PCL/PEO microfibers formed aligned bundles comprising ~4–12 individual filaments. Fiber deposition into bundles is attributed to the low *Z*-axis speed of the collecting frame, which causes fibers to accumulate in the same positions. Thus, the observed spacing should be considered as interbundle spacing rather than interfiber spacing. The interbundle spacing of 91.9 ± 25.0 μm may provide favorable conditions for fibroblast growth, as highlighted in ref. 40 and 41. According to ref. 40, fibroblasts can adhere across a wide range of pore sizes (38–150 μm) within polymer-based scaffolds. Given that the 3T3-GFP cells used in this study have diameters of 15–16 μm, the observed spacing is sufficient to avoid overpopulation and necrotic core formation, while providing optimal voids for cell ECM deposition.

Additional analysis of PCL/PEO fiber morphology using AFM demonstrated a smooth, defect-free fiber surface and an average fiber diameter of 1.9 ± 0.5 μm ($N$ = 30). Representative 2D and 3D images of microfibers within a single bundle are shown in Fig. 2e and f. The obtained diameter is in good agreement with the fiber diameter distribution measured based on SEM imaging.

With the PCL/PEO fiber pattern characteristics established, it becomes possible to estimate the effective fiber surface area as well as the interlayer volume (in 3D scaffolds) available for cell ingrowth. These estimations are summarized in Table 2. The calculation methodology is presented in Table S1 and Scheme S1 (SI).

Touch-spinning of reference PCL solutions produced aligned nanofiber patterns with an average diameter of 376 ± 42 nm and an interfiber spacing of 11.3 ± 2.0 μm. SEM micrographs of the nanofiber patterns, with the corresponding fiber diameter distribution, are shown in Fig. 3. In contrast to PCL/PEO fiber arrays, PCL fibers rarely formed bundles and were deposited individually over short distances, likely due to the higher *Z*-axis speed of the fiber-collecting frame. The combination of solution and technological parameters, including the reduced solution feed rate, favored the formation of nanofibers rather than microfibers. Since the fabricated reference nanofibers are generally more prone to breakage compared with the PCL/PEO fiber patterns, it can be inferred that they provide reduced mechanical support to microscale cells during cell culture. In addition, nanofiber surface defects can be observed in Fig. 3a, where the presence of surface pits indicates active solvent evaporation during the spinning process.

Further, reference PCL touch-spun nanofibers were used to assess crystallinity degree and thermal stability and were not included in the cell culture experiments.

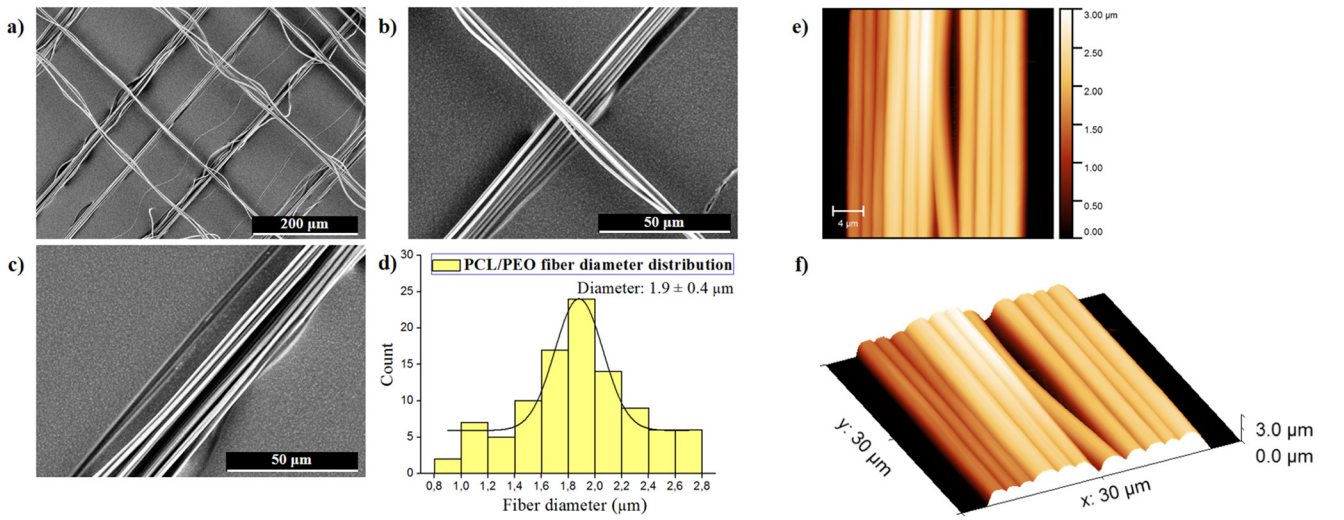


**Fig. 2** PCL/PEO microfiber patterns fabricated from a 5 wt% PCL/0.25 wt% PEO solution *via* the touch-spinning technique at 160–180 rpm and a feed rate of 0.4 mL $h^{-1}$, with a *Z*-axis speed set to 40 mm $h^{-1}$: (a), (b), and (c) SEM images of two orthogonally aligned fiber layers; (d) fiber diameter distribution obtained from SEM data; (e) and (f) 2D and 3D AFM images of the fibers, respectively.

**Table 2** Scaffold geometry, effective surface area, and interlayer volume supporting cell attachment and growth

| | 'Flat surfaces' | Single-layer scaffolds | 3D scaffolds |
|---|---|---|---|
| Scaffold geometry | Square-shaped (22 × 22 mm) film | Planar circular scaffold ($d$ = 19 mm)[a] contains bundles of roughly eight fibers, each 1.9 μm in diameter, with bundles arranged at 91.9 μm intervals | Three single layers stacked with interlayer spacing of ~70 μm |
| Surface area, $mm^2$ | 484.0 | 126.3 | 378.9 |
| Interlayer volume[b], $mm^3$ | — | — | 39.7 |

[a] While cells can potentially grow on the spacer, this scenario is disregarded for our analysis, and only the internal spacer diameter is taken into account. [b] With three stacked fibrous layers, the 3D scaffold forms two cylindrical interlayer voids, each measuring approximately 19.85 $mm^3$ in volume.

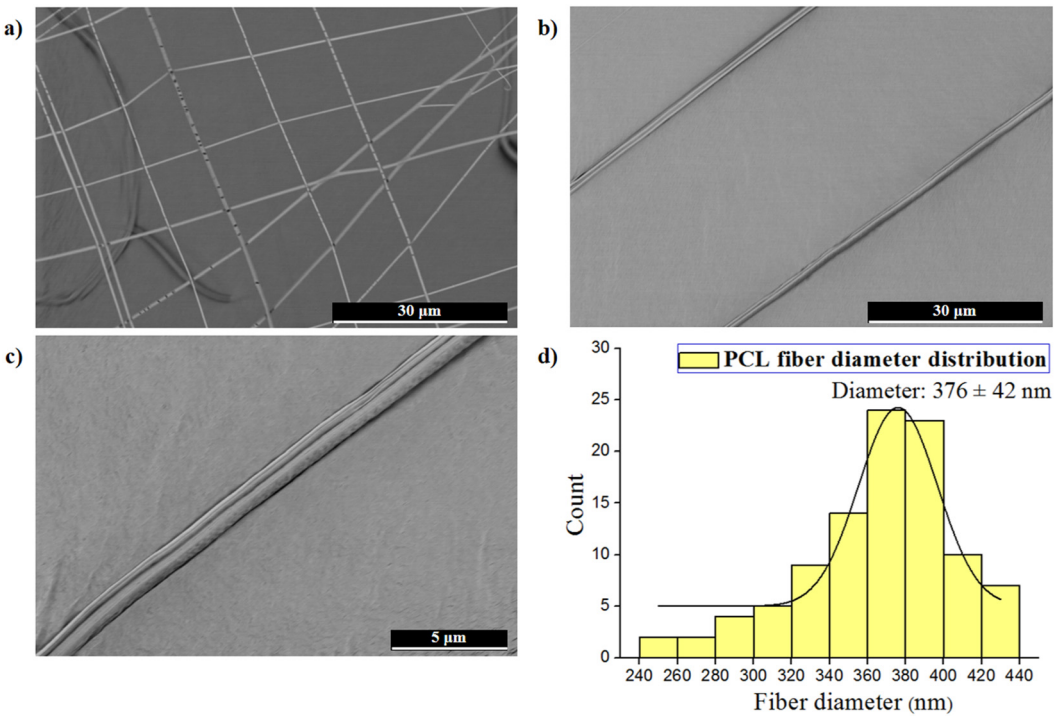


**Fig. 3** Reference PCL nanofiber patterns fabricated from an 8 wt% PCL solution *via* the touch-spinning technique at 140–180 rpm and a feed rate of 0.1 mL $h^{-1}$, with a $Z$-axis speed set to 100 mm $h^{-1}$: (a), (b), and (c) SEM images of two orthogonally aligned fiber layers; (d) fiber diameter distribution obtained from SEM data.

Spun fibers typically exhibit a semicrystalline structure, which plays an important role in biomechanical cell–material interactions and therefore needs to be evaluated. The XRD analysis of PCL/PEO touch-spun microfibers indicates the presence of both polymer phases. The XRD pattern (Fig. 4) displays characteristic (110) and (200) diffraction peaks at 21.5° and 23.7°, corresponding to the orthorhombic crystalline structure of PCL with the $P2_12_12_1$ space group.[42] The other two peaks detected at 19.7° and 22.8° can be attributed to the (120) and (112) crystallographic planes of the water-soluble PEO phase.[43]

In this study, the crystallite size $\langle L\rangle_{hkl}$ of the PCL phase was estimated for the (110) and (200) reflections using eqn (1). The data on peak positions, FWHM, and $\langle L\rangle_{hkl}$ are presented in Table 3.

The average crystallite size determined from the (110) and (200) reflections was found to be ~179.2 Å. Compared with our previous study on the structural characteristics of touch-spun and electrospun PCL nanofibers,[25] the estimated crystallite size is considerably smaller than that reported for touch-spun fibers (311.5 Å). This indicates that the microfibers fabricated within this work may possess enhanced stiffness and an increased surface area, which could influence their biomechanical properties. On the other hand, the crystallite size $\langle L\rangle_{110}$ of ~218.5 Å is slightly larger than the values reported in ref. 42 for aligned PCL nanofibers. The authors suggest that additional stretching forces align extended molecular chains along the fiber axis, allowing them to act as row nuclei for subsequent crystallization. Therefore, the enhanced nucleation leads to a reduced crystallite size $\langle L\rangle_{110}$ of 130 Å.

To further examine the crystalline structure of the touch-spun fibers, the degree of crystallinity of the PCL/PEO microfibers and reference PCL nanofibers was determined by DSC

 

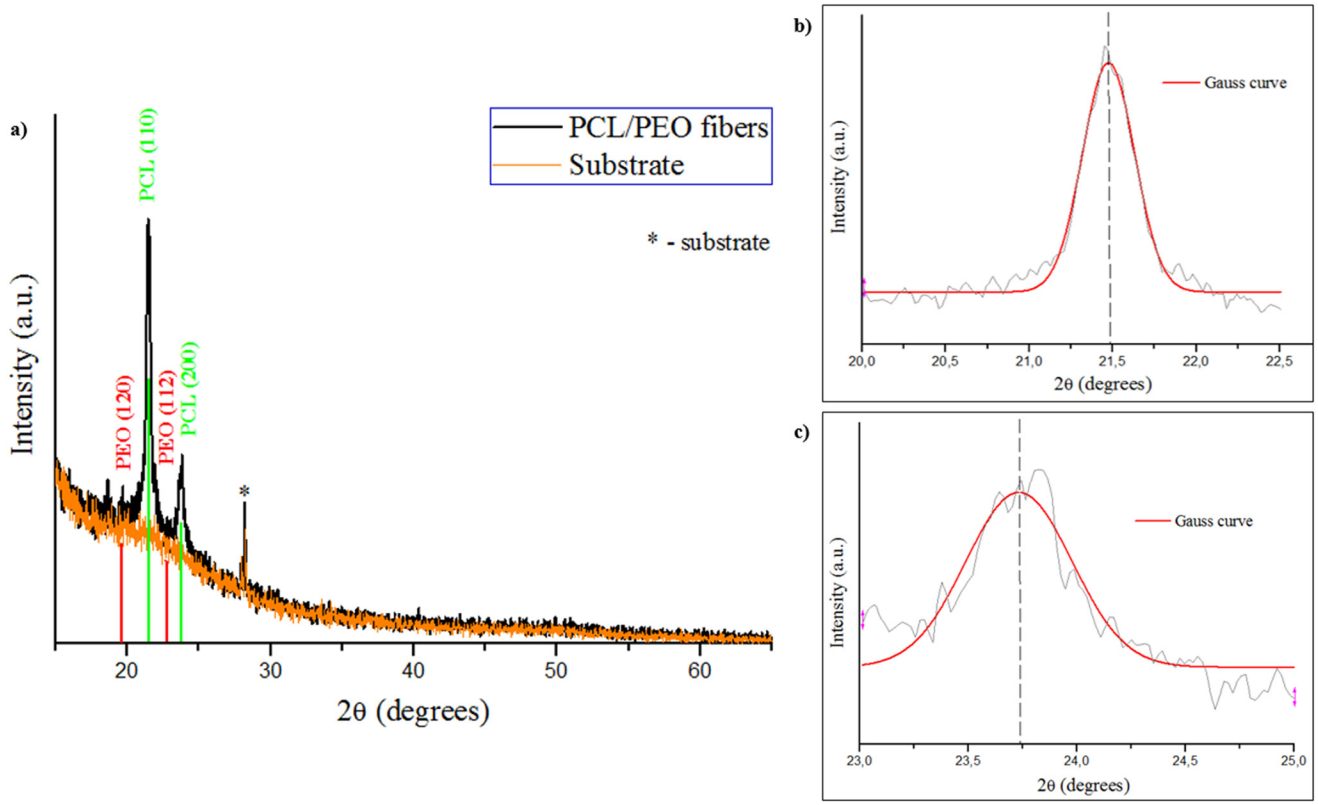


**Fig. 4** XRD analysis of PCL/PEO microfiber crystalline structure: (a) XRD pattern; (b) and (c) analysis of the characteristic diffraction peaks observed for PCL phase at 21.5° and 23.7°, respectively.

**Table 3** Crystallite size estimation using the Debye-Scherrer equation

| Peak position, rad | Crystallographic plane (*hkl*) | FWHM, rad | $\langle L \rangle_{hkl}$, Å |
|---|---|---|---|
| 0.3748 | (110) | 0.0064 | 218.5 |
| 0.4143 | (200) | 0.0100 | 139.9 |

analysis. The DSC analysis was performed using a heating–cooling–heating cycle, and the first melting and crystallization curves of the studied PCL/PEO microfibers are shown in Fig. 5a. As the first heating curves retain the original structural history of the samples, the corresponding melting peaks (Fig. 5b) were used to calculate the degree of crystallinity with high reliability. Table 4 summarizes the degrees of crystallinity determined from the first heating DSC curves (see eqn (2)), alongside the values obtained from XRD analysis.

DSC analysis indicated that the degrees of crystallinity for the touch-spun PCL/PEO microfibers and reference PCL nanofibers were 38.7% and 31.1%, respectively, which is consistent with values reported for electrospun PCL-based nanofibers.[23,44,45] By comparison, touch-spun PCL fibers fabricated at higher rotational speeds (500–2000 rpm) exhibited crystallinity in the range of 54–64%.[23] The reduced crystallinity degree observed in the present study is likely attributed to the lower rotational speeds employed (140–180 rpm), which limit polymer chain stretching and molecular alignment, key factors that promote crystalline ordering in spun fibers. XRD analysis typically yields higher crystallinity values than DSC due to differences in measurement principles. DSC measures the heat absorbed during melting, reflecting only the thermodynamically active crystalline fraction, whereas XRD method detects all long-range ordered regions, including small or defective crystallites that may not melt. Additionally, the thermal history of the sample and overlapping DSC peaks, as observed for the studied PCL/PEO microfibers, can further reduce the apparent crystallinity, while XRD captures the room-temperature structural order.

Fig. 5a and b shows that the touch-spun PCL/PEO microfibers exhibit distinct melting and crystallization peaks at 58.7 °C and 31.5 °C, respectively, characteristic of PCL. In contrast to pure PCL material, the DSC heating curve of the polymer blend also displays a small melting peak at 61.5 °C, corresponding to the melting point of the PEO phase. The glass transition temperature associated with the PCL phase can be observed from the cooling curve (Fig. 5a) at −59.7 °C. According to the thermogram shown in Fig. 5b, the melting point of the PCL/PEO microfibers ($T_m$ = 58.7 °C) is slightly shifted to higher temperatures compared with that of the reference PCL nanofibers ($T_m$ = 54.6 °C). This may indicate a slight stabilization of the scaffold materials upon incorporation of PEO. This higher thermal stability is further confirmed by the

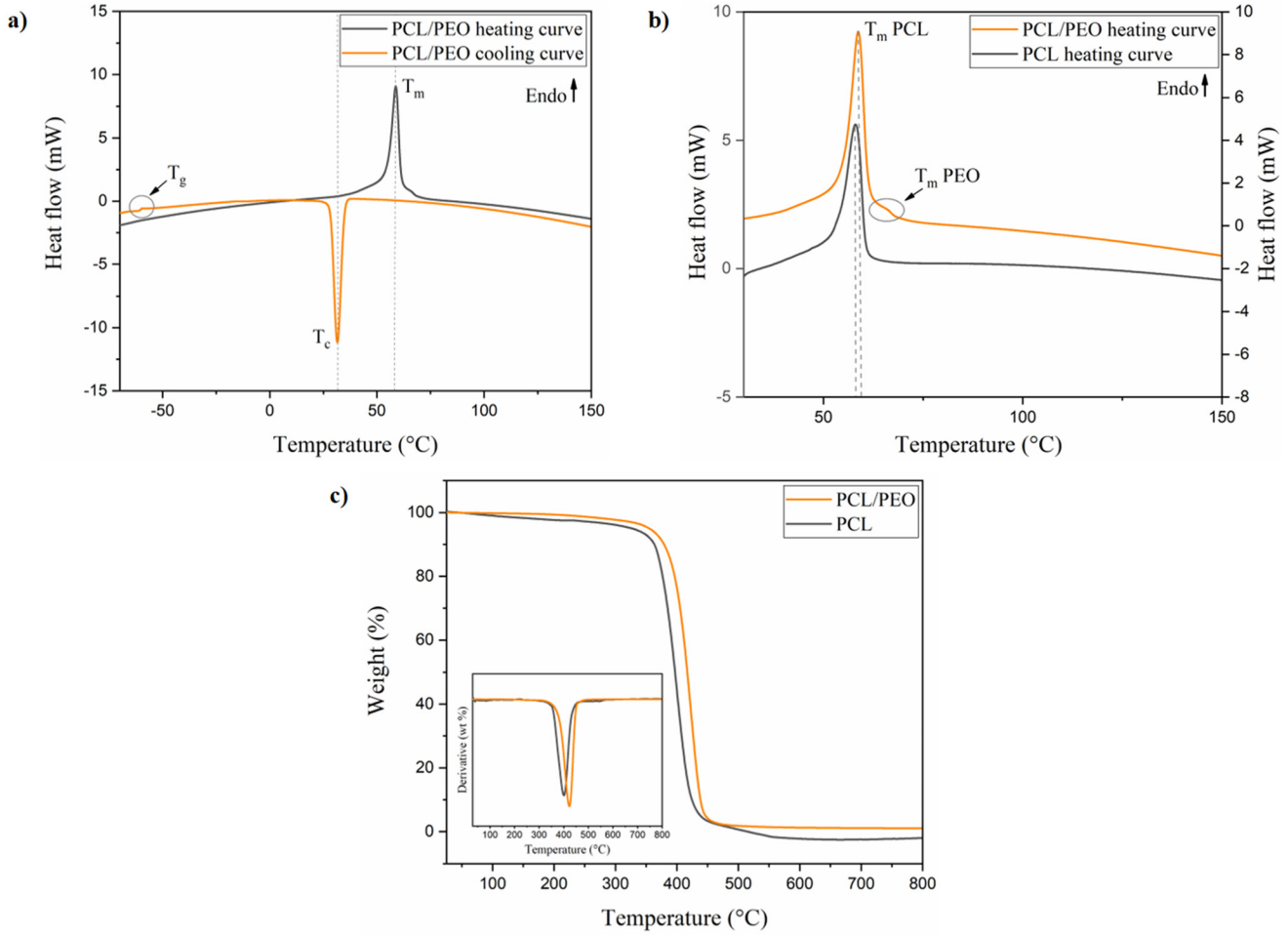


**Fig. 5** Thermal characterization of PCL/PEO microfibers: (a) first heating and cooling DSC thermograms of PCL/PEO microfibers; (b) first heating DSC thermograms of PCL/PEO compared with reference PCL nanofibers; (c) TGA thermograms and corresponding derivative curves (inset) for PCL/PEO microfibers and reference PCL nanofibers.

**Table 4** Degree of fiber crystallinity determined from DSC and XRD analyses

| | $\Delta H_{m1}$, J g$^{-1}$ | | | |
|---|---|---|---|---|
| | PCL | PEO | % Crystallinity (DSC)[a] | % Crystallinity (XRD)[b] |
| PCL/PEO microfibers | 54.2 | 1.7 | 38.7 | 45.9 |
| PCL nanofibers | 43.4 | — | 31.1 | — |

[a] The degree of crystallinity calculated from the DSC curve of PCL/PEO microfibers was corrected for the weight fractions of the individual polymers. [b] The degree of crystallinity determined by XRD was calculated as the ratio of the crystalline peak area to the total area, excluding contributions from substrate reflections. No XRD analysis was performed for the reference PCL nanofibers in this study.

thermogravimetric curves (Fig. 5c), where the onset of degradation of the blend fibers is shifted by 19.4 °C to a higher temperature range, and the total weight loss is reduced by ~4% compared with the pure PCL materials. The slight enhancement in thermal stability of the PCL/PEO touch-spun microfibers can be attributed to the incorporation of high-molecular-weight PEO, which promotes polymer–polymer entanglements and restricts the segmental mobility of PCL chains, thereby delaying thermal degradation and stabilizing the crystalline phase. In addition, the presence of PEO is likely to suppress the recrystallization of ordered domains and the relaxation of oriented amorphous PCL chains, both of which are evidenced by a series of endo- and exothermic peaks in the first heating thermograms of the reference PCL nanofibers in the 0–30 °C temperature range (see Fig. S3, SI).

### 3.2. Study of 3T3 GFP fibroblast activity over a predefined growth duration

Prior to cell culture, three groups of fabricated PCL/PEO scaffolds were treated with vacuum plasma to enhance cell adhesion. The treatment was conducted using air plasma, composed primarily of $N_2$ (~78.08%) and $O_2$ (~20.95%), leading to the generation of reactive nitrogen and oxygen species. These species were expected to functionalize the scaffold surface by introducing polar functional groups,

thereby providing anchoring sites for cell adhesion proteins. Previous studies have demonstrated the effectiveness of atmospheric plasma treatment in modifying electrospun PCL scaffolds.[46–48] Consequently, in this study, plasma treatment was anticipated to enhance fibroblast spreading and promote elongation along the fibers.

GFP-labeled 3T3 fibroblasts were used as the model cell line in this study to facilitate convenient monitoring of cell attachment, spreading, and proliferation by optical microscopy, thereby eliminating the need for an additional Live/Dead staining step to assess cell viability. Additionally, 3T3-GFP fibroblasts are a robust cell line known to exhibit efficient growth on substrates with diverse morphologies. These cells build up ECM, which enables further investigation of cell culture spreading across neighboring fibers in touch-spun scaffold architectures. Illustrative images showing the morphology of fibroblasts used in this study are provided in Fig. 6.

To compare the efficiency of cell growth on PCL/PEO-based scaffolds – 'flat surfaces', single-layer touch-spun scaffolds, and 3D touch-spun scaffolds – 3T3-GFP fibroblasts were seeded on each material group at a density of $\sim 3.8 \times 10^5$ cells per sample using the 'dry' seeding method (see Materials and Methods). This relatively high seeding density was chosen to promote rapid formation of a confluent cell culture. In this experiment, cell cultures were maintained for a 10-day period, and cell viability was assessed on day 3, 5, 7, and 10 using the non-destructive PrestoBlue assay. Following the culture period, terminal MTT and Bradford assays were performed to evaluate cell metabolic activity and cell protein concentration, respectively. Fig. 7 presents the outcomes of the assays.

Based on the PrestoBlue assay, no statistically significant differences in fibroblast viability were observed among the 'flat surface', single-layer scaffold, and 3D scaffold groups at early culture stages. This indicates that shortly after seeding, 3T3-GFP fibroblasts did not establish substantial differences in proliferation pathways across the different culture platforms. The slightly higher mean viability observed for the 3D scaffolds at this time point may reflect early adaptation of fibroblasts to a 3D microenvironment, although this effect was not statistically significant. By day 5, significant differences emerged, with both single-layer and 3D scaffolds exhibiting increased resazurin reduction compared with the 'flat surfaces'. Notably, the 3D scaffolds demonstrated the highest viability, significantly exceeding both other groups. Divergence among culture conditions persisted through days 7 and 10. While conventional 2D substrates showed only modest increase in cell viability, single-layer and 3D scaffolds exhibited substantially higher PrestoBlue signals. The 3D cell cultures consistently produced the highest viability, with statistically significant differences compared with the 'flat surfaces' and, at later time points, the single-layer scaffolds.

MTT test results at the end of the culture period (day 10) revealed that cell metabolic activity was the highest within the 3D scaffolds, with 3T3-GFP cell activity about four times greater than that of the positive control. A statistically significant difference was observed between the 3D scaffolds and both 'flat surfaces' and single-layer scaffolds. In contrast, no significant difference was detected between the two 2D morphologies. Considering both PrestoBlue and MTT outcomes, we assume that cell–cell and cell–material interactions occur more efficiently within the 3D architectures, likely due to enhanced cell signaling. These findings further suggest enhancing cell ECM production, facilitated by a 3D fibrous network that provides optimal interfiber spacing for ECM deposition and supports overall cellular function.

The hypothesis of increased ECM deposition within the 3D scaffolds can be indirectly supported by the cell protein quantification analysis. The Bradford assay showed a similar trend, with 3D scaffolds exhibiting the highest cellular protein content. A significant difference in protein concentration was observed between the 3D scaffolds and both groups of 2D plat-

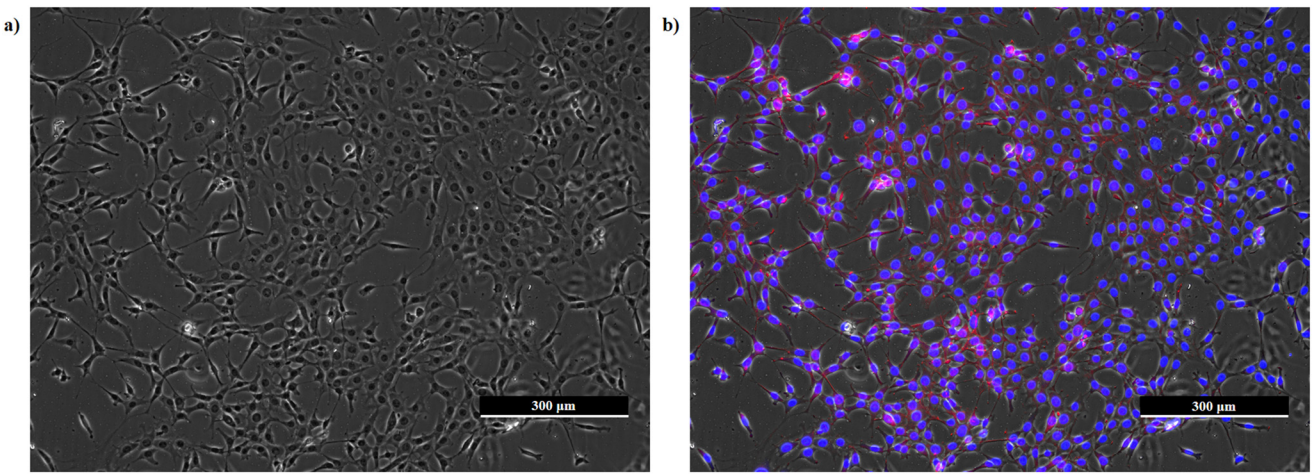


**Fig. 6** Morphology of 3T3-GFP fibroblasts after staining for nuclei (blue) and actin (red). Fluorescence microscopy of cells on a 6-well tissue culture plate (TCP): (a) TRANS channel; (b) merged DAPI, RFP, and TRANS channels.

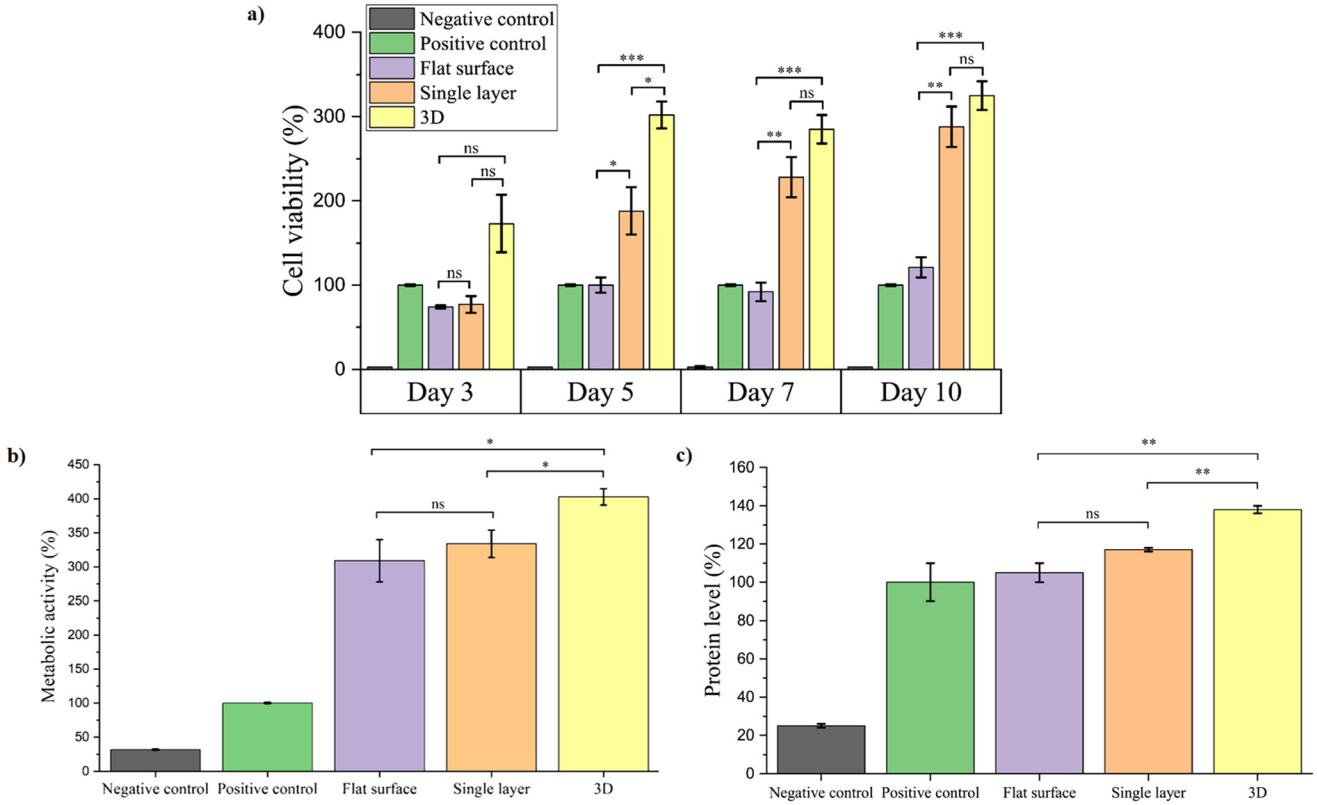


**Fig. 7** Cell-based assays performed for PCL/PEO scaffolds: (a) cell viability assessed by the PrestoBlue assay over a 10-day culture period; (b) cell metabolic activity measured upon completion of culture; and (c) cell protein content evaluated upon completion of culture. Control conditions are described in the Materials and Methods section. Statistical analysis was performed to validate the experimental results, with one-way ANOVA used to determine the significance of differences in cell viability, metabolic activity, and protein content between the scaffold groups.

forms. Based on the BSA calibration curve, protein concentrations per sample were estimated to be 0.32 μg $\mu L^{-1}$, 0.49 μg $\mu L^{-1}$, and 0.81 μg $\mu L^{-1}$ for 'flat surfaces', single-layer scaffolds, and 3D scaffolds, respectively. This further highlights the superior efficiency of 3D scaffolds in supporting cellular protein synthesis.

### 3.3. Assessment of cell growth to high confluency

In the second experiment, 3T3-GFP fibroblasts were seeded on the same three scaffold groups at a density of $5 \times 10^5$ cells per sample using the 'dry' method of seeding. Unlike the first experiment, which followed a fixed culture period, cultures in this study were terminated individually for each scaffold group once apparent cell confluency was observed by fluorescence optical microscopy. The progression of cell growth on 'flat surfaces', single-layer scaffolds, and 3D scaffolds is shown in Fig. 8, 9, and 10, respectively. At the end of the culture period, cells on the scaffolds were stained for nuclei and actin to facilitate visualization.

Although cells were seeded at the same density on all three scaffold groups, the time required to reach maximum cell confluency, as assessed by optical microscopy, varied significantly. Thus, for 3T3-GFP fibroblasts seeded onto polymer films at a density of $5 \times 10^5$ cells per sample, maximum confluency was reached rapidly, with cells completely covering the substrate surface by day 3. Furthermore, once maximum confluency is achieved on conventional 2D substrates, cells tend to form a monolayer (sheet) that may begin to detach from the material. This behavior was observed for several 'flat surfaces' examined in this study (Fig. S4, SI).

In contrast to polymer films, fibroblast growth on single-layer touch-spun scaffolds occurred over a more extended period, with cells fully occupying the microfibers and interfiber spacing by day 11. Notably, no cell sheet detachment was observed for these 2D fibrous substrates. This indicates that single-layer touch-spun scaffolds are more effective in maintaining dense cell cultures. The fibrous network prevents rapid overconfluency and provides pathways for nutrient transport. Fig. 9a shows that 3T3-GFP fibroblasts tend to elongate along the fiber axis, a behavior that is evident from the early stages of cell culture. This alignment may result from the high affinity of the cells for PCL/PEO material, as well as surface functionalization of the fibers induced by air plasma treatment. Moreover, it has been hypothesized[25] that the alignment may be influenced by the specific degree of crystallinity of touch-spun fibers. Higher crystallinity could induce the arrangement of actin filaments and activation of regulatory proteins (Rac1 and Cdc42). These proteins, in

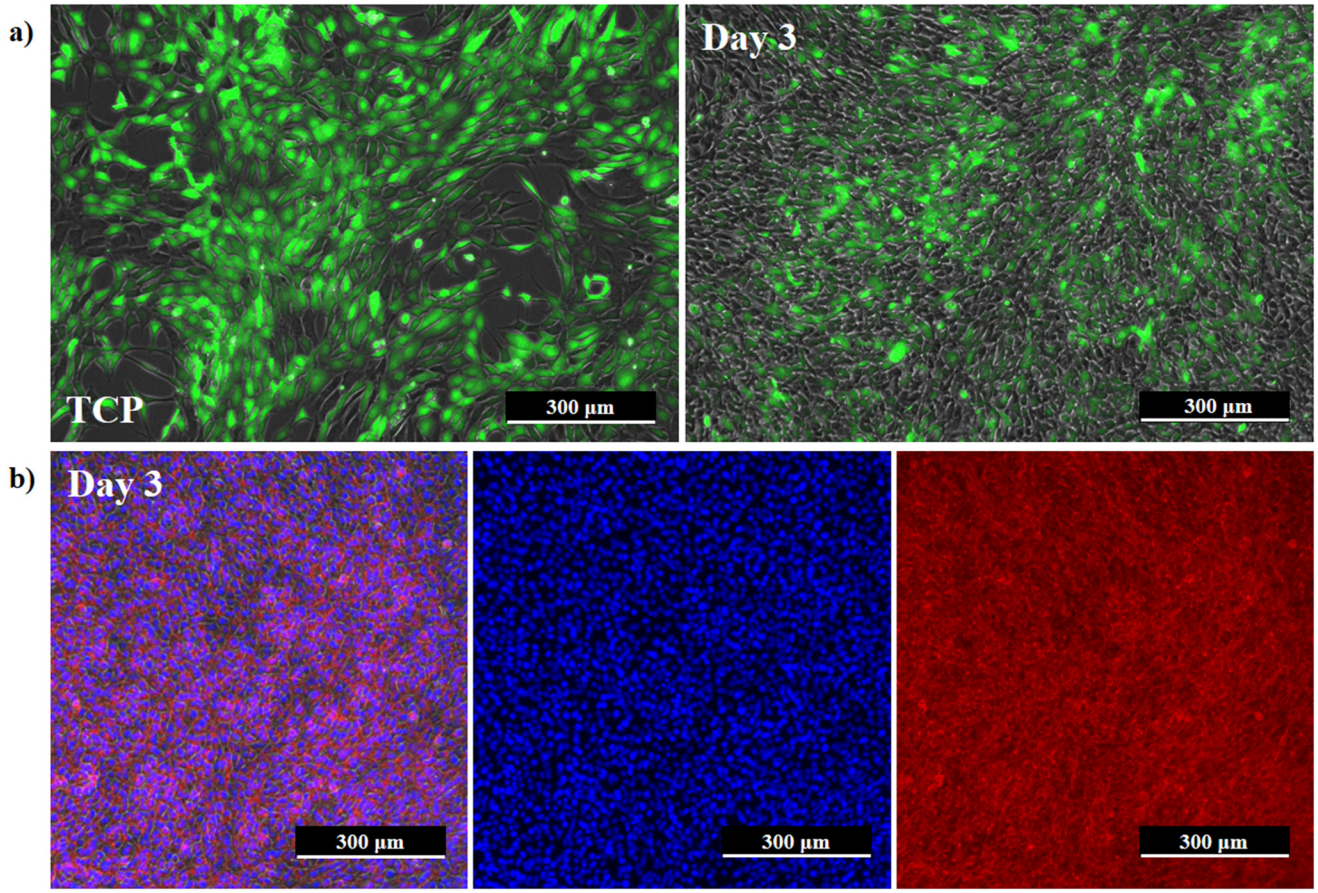


**Fig. 8** Progression of cell growth on PCL/PEO films ('flat surfaces'): (a) fluorescence microscopy images (merged TRANS and GFP channels) showing 3T3-GFP fibroblasts on TCP prior to seeding (left) and a confluent cell layer on 'flat surfaces' achieved by day 3 (right); (b) fluorescence microscopy images of cells stained for nuclei (blue) and actin (red) after maximum confluency was reached. From left to right: merged DAPI and RFP channels, DAPI channel, and RFP channel.

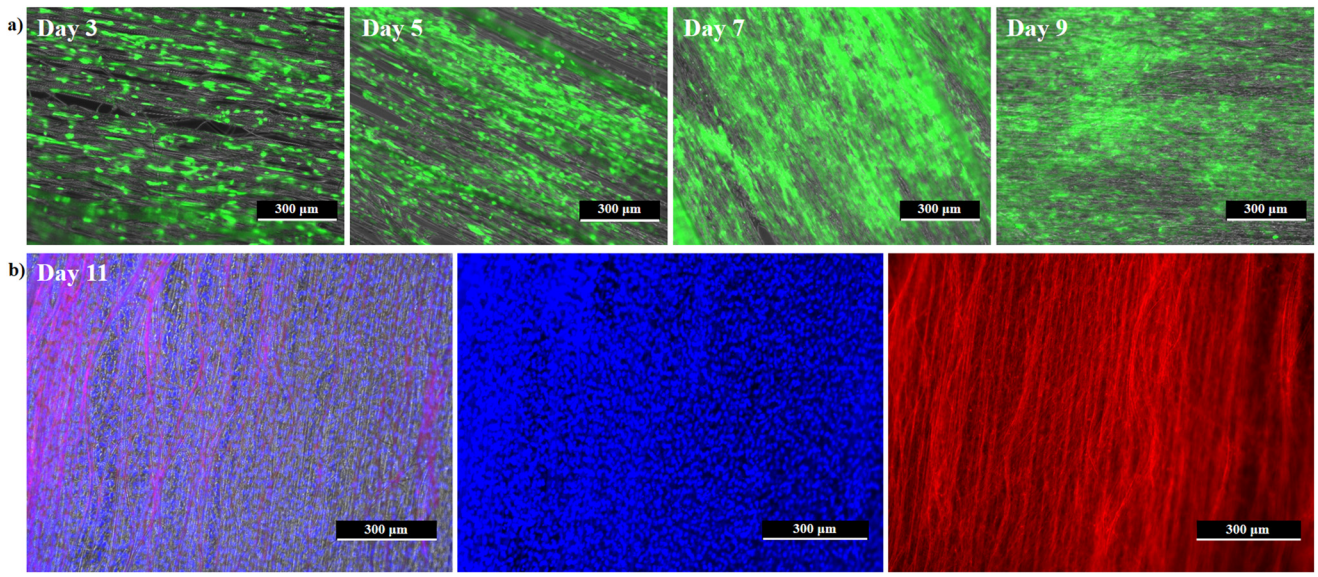


**Fig. 9** Progression of cell growth on PCL/PEO single-layer scaffolds: (a) fluorescence microscopy images (merged TRANS and GFP channels) showing 3T3-GFP fibroblast growth up to day 9; (b) fluorescence microscopy images of cells stained for nuclei (blue) and actin (red) on day 11. From left to right: merged DAPI and RFP channels, DAPI channel, and RFP channel.

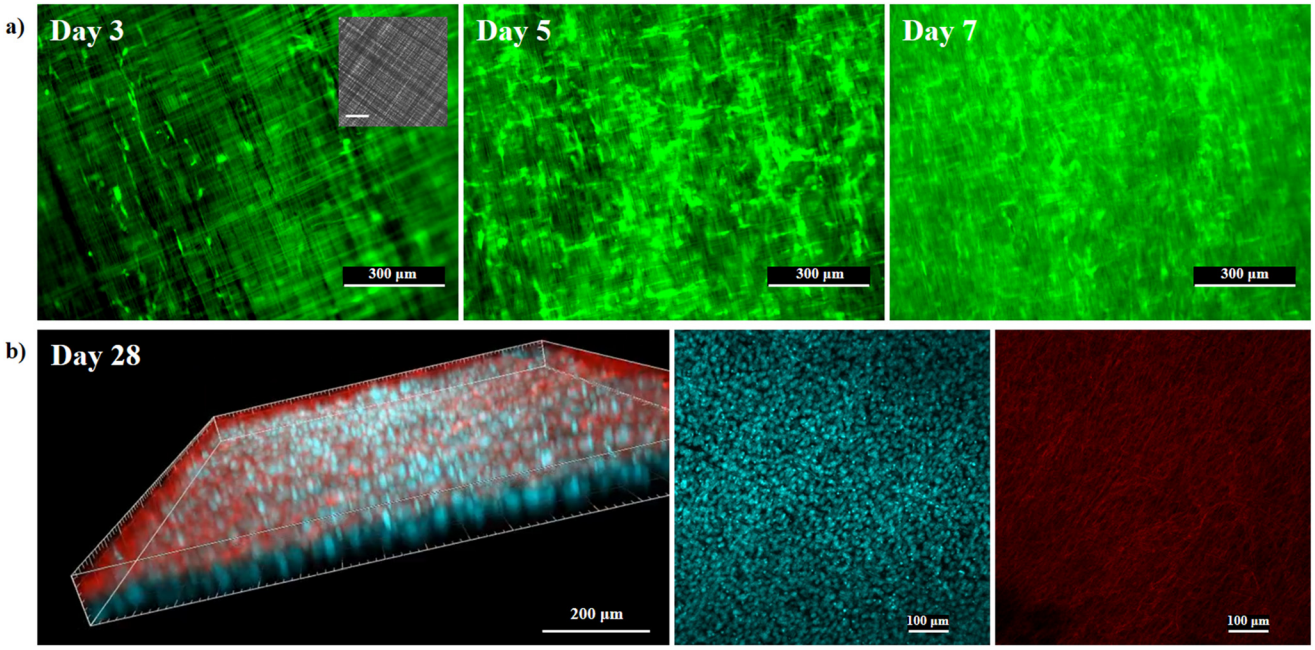


**Fig. 10** Progression of cell growth on PCL/PEO 3D scaffolds: (a) fluorescence microscopy images (GFP channel) showing 3T3-GFP fibroblast growth up to day 7 (the inset scale bar is 750 μm); (b) confocal microscopy images of cells stained for nuclei (blue) and actin (red) on day 21. From left to right: 3D image of the scaffold obtained *via Z*-stacking in merged DAPI and RFP channels, projection of the scaffold area in DAPI channel, and projection of the scaffold area in RFP channel.

turn, participate in the phosphorylation of cell proliferation regulators, including YAP1, ultimately contributing to directed cell growth.

For 3D touch-spun scaffolds, cultures were maintained for 21 days, at which point growth was halted upon detection of regions exhibiting local overpopulation. Due to overlapping signals from different scaffold layers, standard optical microscopy tools do not allow for accurate determination of the time required to reach maximum confluency. Therefore, after approximately seven days of cell culture, standard imaging is impeded, requiring confocal microscopy to visualize cells within the scaffold.

Uneven cell distribution across scaffold layers complicates estimation of both maximum scaffold capacity to support healthy cell growth and the time required to reach full confluency. Some layers remain sparsely populated, while others become densely overcrowded with cells, potentially resulting in the formation of early necrotic cores. Furthermore, when cell growth predominantly progresses from the bottom layer – where most cells are initially captured – to the upper layers, fibroblasts with diameters of ~15–16 μm require sufficient time to fully span the interlayer distances (~60–80 μm). Fig. 10b shows a 3D image of the scaffold after 21 days of culture, obtained by *Z*-stack projection with a stacking depth of ~183 μm. Both the 3D image and scaffold area projections indicate the formation of dense cell cultures throughout the scaffold architecture. Based on confocal microscopy observations, no necrotic cores were detected within the structure. However, layer-by-layer analysis is hindered by the high fluorescence intensity originating from the stained dense cell cultures. Additional 3D illustration of the scaffold is provided in Fig. S5 and Video S1 (SI).

Thus, healthy 3T3-GFP fibroblast growth on 3D touch-spun scaffolds was maintained for up to 21 days, compared with the first two scaffold groups, and could potentially be extended further if monitoring of cell growth within individual layers and interlayer voids is optimized.

For touch-spun scaffolds, fibroblast cells follow a characteristic proliferation pattern, as shown in Fig. 11a, which depicts cell proliferation across two orthogonally aligned microfiber layers. Cells preferentially occupy the edges of rectangular voids, particularly at fiber intersection points where mechanical support is optimal. As culture time progresses, cells continue to populate the voids, spreading from the edges toward the centers. Thus, the voids adopt a circular morphology until they are fully occupied by cells. Fig. 11b illustrates cell cross-adhesion between adjacent microfibers. This observation demonstrates the ability of 3T3-GFP fibroblasts to proliferate by depositing ECM within the interfiber spacing, utilizing the fibers as mechanical support points.

To quantify the number of 3T3-GFP fibroblasts supported by the scaffolds, we performed cell counting using the standard trypsinization method. Cells were harvested on day 3, 11, and 21 from 'flat surfaces', single-layer scaffolds, and 3D scaffolds, respectively. During the cell counting procedure, we continued harvesting cells until optical microscopy

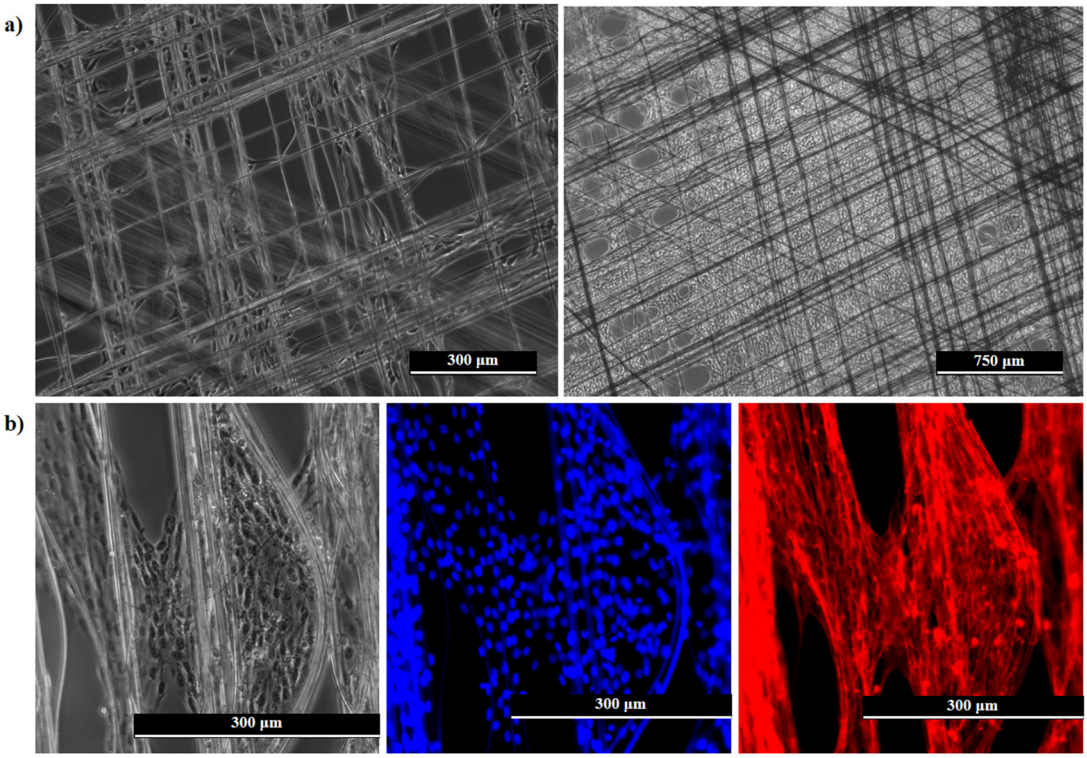


**Fig. 11** 3T3-GFP fibroblast growth characteristics: (a) fluorescence microscopy images (TRANS channel) showing cell spreading across two orthogonally aligned microfiber layers at early (left) and later (right) stages of culture; (b) fluorescence microscopy images of cell cross-adhesion between adjacent microfibers after cell staining. From left to right: TRANS, DAPI, and RFP channels.

showed no cells or only a few remaining on the material. Since the three groups of materials have different morphologies, we varied the number of trypsinization and PBS washing rounds accordingly: for 'flat surfaces', we performed one trypsinization with a single PBS wash; for single-layer scaffolds, we performed one trypsinization followed by three PBS washes; and for 3D scaffolds, we performed two trypsinization rounds, each followed by two to three PBS washes. To avoid counting damaged cells, we disregarded all cells with diameters under 8 µm, which likely corresponded to dead cells or organoids resulting from prolonged exposure to trypsin. The outcomes of the cell harvesting experiments are presented in Table 5.

The outcomes of the cell counting procedure conducted with cell harvesting indicate that 3D fiber structures support the highest number of cells. The maximum number of fibroblasts harvested from the 3D scaffold was $6.450 \times 10^6$ (SI, Fig. S6). However, the average cell count obtained for 3D scaffolds was lower than the theoretical maximum, suggesting uneven cellular coverage across the three layers and interlayer spacing. In contrast, single-layer scaffolds exhibited significantly higher cell counts compared with polymer films (SI, Fig. S7). This difference may be attributed to the fact that single-layer scaffolds do not function as purely 2D substrates; the presence of multiple fibers not aligned in the same plane creates additional directions for cell growth. Deviations from an ideal planar structure can arise from technological imperfections, such as deformed spacers or overlapping fiber arrays. The slight decrease in the average cell number observed for conventional 2D substrates reflects initial cell loss (~10%) occurring during seeding.

Overall, comparison of cell numbers across the three scaffold groups demonstrates the superior capacity of 3D touch-spun scaffolds to sustain dense cell cultures over extended periods, in agreement with the cell viability and metabolic activity results reported earlier in this study.

**Table 5** Cell counting of harvested cells across three scaffold groups[a]

| | Average cell number (trypsinization) | Average cell number (MTT curve) | Minimum detected cell diameter, µm |
|---|---|---|---|
| 'Flat surfaces' (day 3) | $4.470 \times 10^5$ | $7.570 \times 10^5$ | 14.5 |
| Single-layer scaffolds (day 11) | $2.377 \times 10^6$ | $2.672 \times 10^6$ | 13.0 |
| 3D scaffolds (day 21) | $5.300 \times 10^6$ | $5.082 \times 10^6$ | 9.8 |

[a] Cell diameter distribution histograms are presented in Fig. S6 and S7 (SI).

## 4. Conclusions

This study presents a comparative analysis of three groups of PCL/PEO-based cell culture platforms: conventional 2D sub-

strates, 2D touch-spun scaffolds, and 3D touch-spun scaffolds, designed for long-term cell culture in tissue engineering. Leveraging the new touch-spinning technique, we produced aligned nano- and microfiber arrays with uniform interfiber/interbundle spacing, providing structural cues optimal for fibroblast proliferation. For reference nanofibers, we achieved a diameter of 376 ± 42 nm and an interfiber spacing of 11.3 ± 2.0 μm, while for studied microfiber patterns, the diameter was 1.9 ± 0.4 μm and interbundle spacing was 91.9 ± 25.0 μm. Comparative biological evaluations revealed that the 3D touch-spun scaffolds significantly outperformed 2D substrates, exhibiting enhanced cell viability, metabolic activity, and total protein content as confirmed by PrestoBlue, MTT, and Bradford assays over a 10-day culture period. Importantly, the 3D platforms maintained a robust population of up to ~6.5 million 3T3-GFP fibroblasts and supported culture durations of up to 21 days – substantially longer than most previously reported cell culture studies, which typically do not exceed one week. These findings underscore the critical role of scaffold architecture in directing cell behavior. The underexplored structural features of touch-spun fibers, particularly crystallinity, alignment, and mechanical strength, appear to enhance biomechanical signaling in 3D environments, contributing to sustained cell proliferation. 3D microfibrous architectures provide additional biomechanical cues for cell attachment, proliferation, and enhanced cell ECM deposition. Our observations during culture further revealed cell elongation along fiber axes and preferred population in interfiber voids at fiber intersection points, where mechanical support is optimal. We envision future studies that will focus on the influence of scaffolds' structural and mechanical characteristics on proliferation mechanisms and explore the applicability of this platform across additional cell types. Altogether, this work demonstrates the potential of 3D touch-spun scaffolds as advanced culture platforms capable of supporting long-term growth and may inform future designs of bioengineered tissues and regenerative systems.

## Author contributions

KP: conceptualization, data curation, formal analysis, investigation, methodology, visualization, writing – original draft, and writing – review & editing. MP: investigation, and visualization. MA: investigation, data curation, visualization, methodology, writing – original draft, and writing – review & editing. PV: investigation. SM: investigation, and methodology. NSY: methodology, supervision. SM: project administration, methodology, supervision, and writing – review & editing. VR: project administration, supervision, methodology, and writing – review & editing.

## Conflicts of interest

The authors declare no competing financial interest.

## Data availability

The data supporting this article have been included as part of the supplementary information (SI). Supplementary information: Fig. S1–S7, Video S1, Scheme S1, and further experimental details about the used materials, their characterization, and cell imaging. See DOI: https://doi.org/10.1039/d5nr05509a.

## Acknowledgements

This research was partially funded by the Georgia Research Alliance under Grant No. RGRA1000174300A. M. A. acknowledges support by the U.S. Department of Energy, Office of Science, Office of Biological and Environmental Research program under Award No. DE-SC0023338. N. S. Y. acknowledges support from the USDA National Institute of Food and Agriculture STTR Program, USA (Grant No. 2023-51402-39329), and the Good Food Institute (Grant Title: Tailored, Edible, and Scalable 3D Fiber Scaffolds for Shrimp Cell Expansion). K. P. and V. R. express their gratitude to Dr Vladislav Klepov for assistance in XRD analysis. K. P. expresses her gratitude to Dr Eric Formo for assistance in SEM imaging.

## References

1 W. Li, *et al.*, Fine-tuning of porous microchannelled silk fibroin scaffolds for optimal tissue ingrowth, *Mater. Des.*, 2025, **251**, 113711.
2 J. L. Lowery, N. Datta and G. C. Rutledge, Effect of fiber diameter, pore size and seeding method on growth of human dermal fibroblasts in electrospun poly (ε-caprolactone) fibrous mats, *Biomaterials*, 2010, **31**(3), 491–504.
3 S. Soliman, *et al.*, Controlling the porosity of fibrous scaffolds by modulating the fiber diameter and packing density, *J. Biomed. Mater. Res., Part A*, 2011, **96**(3), 566–574.
4 J. Dolgin, *et al.*, Mechanical properties and morphological alterations in fiber-based scaffolds affecting tissue engineering outcomes, *Fibers*, 2023, **11**(5), 39.
5 T. Górnicki, *et al.*, Biomimetic Scaffolds—A Novel Approach to Three Dimensional Cell Culture Techniques for Potential Implementation in Tissue Engineering, *Nanomaterials*, 2024, **14**(6), 531.
6 E. Rosellini, *et al.*, Biomimetic approaches in scaffold-based blood vessel tissue engineering, *Biomimetics*, 2024, **9**(7), 377.
7 J. K. Kular, S. Basu and R. I. Sharma, The extracellular matrix: Structure, composition, age-related differences, tools for analysis and applications for tissue engineering, *J. Tissue Eng.*, 2014, **5**, 2041731414557112.
8 P. Li, *et al.*, Aligned fibrous scaffolds promote directional migration of breast cancer cells via caveolin-1/YAP-mediated mechanosensing, *Mater. Today Bio*, 2024, **28**, 101245.

9 F. Urciuolo, G. Imparato and P. Netti, In vitro strategies for mimicking dynamic cell–ECM reciprocity in 3D culture models, *Front. Bioeng. Biotechnol.*, 2023, **11**, 1197075.
10 W.-H. Han, *et al.*, Electrospun aligned nanofibers: A review, *Arabian J. Chem.*, 2022, **15**(11), 104193.
11 A. J. Robinson, *et al.*, Comparative analysis of fiber alignment methods in electrospinning, *Matter*, 2021, **4**(3), 821–844.
12 K. Zhang, *et al.*, A new magnetic melt spinning device for patterned nanofiber, *Sci. Rep.*, 2021, **11**(1), 8895.
13 D. Jao, X. Hu and V. Beachley, Bioinspired silk fiber spinning system via automated track-drawing, *ACS Appl. Bio Mater.*, 2021, **4**(12), 8192–8204.
14 A. S. Nain, *et al.*, Control of cell behavior by aligned micro/nanofibrous biomaterial scaffolds fabricated by spinneret–based tunable engineered parameters (STEP) technique, *Small*, 2008, **4**(8), 1153–1159.
15 A. S. Nain, *et al.*, Dry spinning based spinneret based tunable engineered parameters (STEP) technique for controlled and aligned deposition of polymeric nanofibers, *Macromol. Rapid Commun.*, 2009, **30**(16), 1406–1412.
16 A. Tokarev, *et al.*, Touch-and brush-spinning of nanofibers, *Adv. Mater.*, 2015, **27**(41), 6526–6532.
17 J. Wang and A. S. Nain, Suspended micro/nanofiber hierarchical biological scaffolds fabricated using non-electrospinning STEP technique, *Langmuir*, 2014, **30**(45), 13641–13649.
18 Q. Hao, *et al.*, Gravity-Driven Ultrahigh-Speed Electrospinning for the Production of Ethyl Cellulose Fibers with Tunable Porosity for Oil Absorption, *ACS Sustainable Chem. Eng.*, 2024, **13**(1), 507–517.
19 N. S. Yadavalli, *et al.*, Gravity Drawing of Micro–and Nanofibers for Additive Manufacturing of Well–Organized 3D–Nanostructured Scaffolds, *Small*, 2020, **16**(11), 1907422.
20 M. A. Obeid, *et al.*, Formulation of polycaprolactone meshes by melt electrospinning for controlled release of daunorubicin in tumour therapy, *Colloids Surf., A*, 2024, **699**, 134873.
21 D. Li, *et al.*, Preparation and Characterization of Novel Multifunctional Wound Dressing by Near-Field Direct-Writing Electrospinning and Its Application, *Polymers*, 2024, **16**(11), 1573.
22 L. F. Deravi, *et al.*, Design and fabrication of fibrous nanomaterials using pull spinning, *Macromol. Mater. Eng.*, 2017, **302**(3), 1600404.
23 D. Asheghali, *et al.*, Enhanced neuronal differentiation of neural stem cells with mechanically enhanced touch-spun nanofibrous scaffolds, *Nanomedicine*, 2020, **24**, 102152.
24 M. Cavanaugh, *et al.*, Influence of touch-spun nanofiber diameter on contact guidance during peripheral nerve repair, *Biomacromolecules*, 2022, **23**(6), 2635–2646.
25 S.-J. Lee, *et al.*, Touch-spun nanofibers for nerve regeneration, *ACS Appl. Mater. Interfaces*, 2019, **12**(2), 2067–2075.
26 W. Kitana, *et al.*, Biofabrication of Composite Bioink-Nanofiber Constructs: Effect of Rheological Properties of Bioinks on 3D (Bio)Printing and Cells Interaction with Aligned Touch Spun Nanofibers, *Adv. Healthcare Mater.*, 2023, **13**(6), 2303343.
27 J. Uribe-Gomez, *et al.*, Soft elastic fibrous scaffolds for muscle tissue engineering by touch spinning, *ACS Appl. Bio Mater.*, 2021, **4**(7), 5585–5597.
28 J. Uribe-Gomez, *et al.*, Fibrous Scaffolds for Muscle Tissue Engineering Based on Touch–Spun Poly (Ester–Urethane) Elastomer, *Macromol. Biosci.*, 2022, **22**(4), 2100427.
29 M. F. Ismail, *et al.*, High–Throughput Production of Gelatin–Based Touch–Spun Nanofiber for Biomedical Applications, *Adv. Eng. Mater.*, 2024, **26**(23), 2401022.
30 K. Y. DeLeon-Pennell, T. H. Barker and M. L. Lindsey, Fibroblasts: The arbiters of extracellular matrix remodeling, *Matrix Biol.*, 2020, **91**, 1–7.
31 J. Franco-Barraza, *et al.*, Preparation of extracellular matrices produced by cultured and primary fibroblasts, *Curr. Protoc. Cell Biol.*, 2016, **71**(1), 10.9.1–10.9.34.
32 K. Peranidze, *et al.*, Strategies for fabricating aligned nano- and microfiber scaffolds: an overview for cell culture applications, *Nanoscale*, 2025, **17**(36), 20670–20703.
33 M. Parker, *et al.*, Insulin-producing INS-1 cell cultures on biomimetic 3D scaffolds, *J. Mater. Chem. B*, 2025, **13**(38), 12134–12145.
34 M. M. Uddin, *et al.*, Fabrication of Aligned Polyhydroxybutyrate Fibrous Scaffolds via a Touchspinning Apparatus, *ACS Omega*, 2025, **10**(22), 22735–22746.
35 K. Peranidze, T. V. Safronova and N. R. Kildeeva, Fibrous polymer-based composites obtained by electrospinning for bone tissue engineering, *Polymers*, 2021, **14**(1), 96.
36 A. Fernandez-Tena, *et al.*, Effect of Molecular Weight on the Crystallization and Melt Memory of Poly (ε-caprolactone)(PCL), *Macromolecules*, 2023, **56**(12), 4602–4620.
37 D. N. Karmalkar, *et al.*, Electrochemical Performance of PEO–NaNO3—NASICON Polymer–Ceramic Composite Electrolytes: The Roles of Composition and Particle Size of Ceramic Filler, *J. Phys. Chem. C*, 2025, **129**(46), 20495–20505.
38 P. Vertegel, *et al.*, Cell detachment: A review of techniques, challenges, and opportunities for advancing biomedical research and applications, *Prog. Biophys. Mol. Biol.*, 2025, **196**, 50–68.
39 H. Yuan, *et al.*, Stable jet electrospinning for easy fabrication of aligned ultrafine fibers, *J. Mater. Chem.*, 2012, **22**(37), 19634–19638.
40 F. J. O'Brien, *et al.*, The effect of pore size on cell adhesion in collagen-GAG scaffolds, *Biomaterials*, 2005, **26**(4), 433–441.
41 K. Peranidze, T. V. Safronova and N. R. Kildeeva, Electrospun nanomaterials based on cellulose and its derivatives for cell cultures: recent developments and challenges, *Polymers*, 2023, **15**(5), 1174.
42 X. Wang, *et al.*, Crystalline morphology of electrospun poly (ε-caprolactone)(PCL) nanofibers, *Ind. Eng. Chem. Res.*, 2013, **52**(13), 4939–4949.
43 M. Basappa, *et al.*, Preparation, characterization, and electrochemical properties of PEO/PVDF blend films, *Chem. Phys. Lett.*, 2022, **799**, 139609.

44 M. D. Flamini, *et al.*, Annealing post-drawn polycaprolactone (PCL) nanofibers optimizes crystallinity and molecular alignment and enhances mechanical properties and drug release profiles, *Mater. Adv.*, 2022, **3**(7), 3303–3315.
45 S.-C. Wong, A. Baji and S. Leng, Effect of fiber diameter on tensile properties of electrospun poly (ε-caprolactone), *Polymer*, 2008, **49**(21), 4713–4722.
46 A. Esmaeili Ranjbar, *et al.*, Surface modification of electrospun polycaprolactone and zein using cold atmospheric plasma for tissue engineering applications, *Sci. Rep.*, 2025, **15**(1), 14567.
47 H. Turkoglu Sasmazel, M. Alazzawi and N. Kadim Abid Alsahib, Atmospheric pressure plasma surface treatment of polymers and influence on cell cultivation, *Molecules*, 2021, **26**(6), 1665.
48 J. Yan, *et al.*, Effect of atmospheric pressure plasma jet treatment on the performance of needleless electrostatic spinning with low concentration of PCL solution, *J. Text. Inst.*, 2025, **116**(2), 328–337.